Approximating 3D bedrock deformation in an Antarctic ice-sheet model for sea-level projections

Caroline J. van Calcar[1,2], Pippa L. Whitehouse[3], Roderik S.W. van de Wal[1,4] & Wouter van der Wal[2]
[1]Institute for Marine and Atmospheric research Utrecht, Utrecht University, Utrecht, 3508 TA, The Netherlands
[2]Faculty of Aerospace Engineering, Delft University of Technology, Delft, 2629 HS, The Netherlands
[3]Department of Geography, Durham University, Durham, UK
[4]Department of Physical Geography, Utrecht University, Utrecht, 3584 CB, The Netherlands

Correspondence to: Caroline J. van Calcar (c.j.vancalcar@uu.nl)

Abstract. The bedrock deformation in response to a melting ice sheet provides a negative feedback on ice mass loss. When modelling the future behaviour of the Antarctic Ice Sheet, the impact of bed deformation on ice dynamics varies but can reduce projections of future sea-level rise by up to 40% in comparison with scenarios that assume a rigid Earth. The rate of the solid Earth response is mainly dependent on the viscosity of the Earth's mantle, which varies laterally and radially with several orders of magnitude across Antarctica. Because modelling the response for a varying viscosity is computationally expensive and has only recently been shown to be necessary over centennial time scales, sea-level projection ensembles often exclude the Earth's response or apply a globally constant relaxation time or viscosity. We use a coupled model to investigate the accuracy of various approaches to modelling the bedrock deformation to ice load change. Specifically, we compare the sea level projections from an ice-sheet model coupled to (i) an elastic lithosphere, relaxed asthenosphere (ELRA) model, with either uniform and laterally varying relaxation times, (ii) a glacial isostatic adjustment (GIA) model with a radially varying Earth structure (1D GIA model), and (iii) a GIA model with laterally varying earth structures (3D GIA model). Furthermore, using the 3D GIA model we determine a relation between relaxation time and viscosity which can be used in ELRA and 1D models. We conduct 500 year projections of Antarctic Ice Sheet evolution using two different climate models and two emissions scenarios: the high emission scenario SSP5-8.5 and the low emission scenario SSP1-2.6. The results show that using a uniform relaxation time of 300 years in an ELRA model leads to a total sea-level rise that deviates less than 40 cm (6%) from the average of the 3D GIA models in 2500. This difference in the projected sea-level rise can be further reduced to 20 cm (4%) by using an upper mantle viscosity of 10^{19} Pa·s in the 1D GIA model, and to 10 cm (2%) in 2500 by using a laterally varying relaxation time map in an ELRA model. Our results show that the Antarctic Ice Sheet contribution to sea-level rise can be approximated sufficiently accurate using ELRA or a 1D GIA model when the recommended parameters derived from the full 3D GIA model are used.

heeft verwijderd: ice sheet –
heeft verwijderd: interaction
heeft verwijderd:
heeft opmaak toegepast: Engels (Verenigd Koninkrijk)
heeft opmaak toegepast: Engels (Verenigd Koninkrijk)
heeft opmaak toegepast: Engels (Verenigd Koninkrijk)
heeft opmaak toegepast: Engels (Verenigd Koninkrijk)
heeft verwijderd: accounting for
heeft verwijderd: predictions
heeft verwijderd:
heeft verwijderd: complex
heeft verwijderd:
heeft verwijderd: projections
heeft verwijderd: ,
heeft verwijderd: We
heeft verwijderd: how accurate such approximations are usin ice sheet model coupled with a glacial isostatic adjustment (GIA) model that simulates
heeft verwijderd: response to changes in ice loading includin lateral and radial variations in viscosity (3D GIA model). Using t 3D model
heeft verwijderd: determined a relation between relaxation ti and viscosity which can be used in simpler models. We
heeft verwijderd: output
heeft verwijderd: and
heeft verwijderd:) and a 3D
heeft verwijderd: . We conducted
heeft verwijderd: the
heeft verwijderd: ice sheet
heeft verwijderd: the
heeft verwijderd: or an upper mantle viscosity of 10^{19} Pa·s in 1D GIA model
heeft verwijderd:
heeft verwijderd:
heeft verwijderd: predicted with 1D and 3D GIA models
heeft verwijderd: 10
heeft verwijderd: maps
heeft verwijderd: effect of 3D viscosity variations on the AIS
heeft verwijderd:
heeft verwijderd: the
heeft verwijderd: model

1 Introduction

The Antarctic Ice Sheet (AIS) might contribute several meters to global mean sea-level rise by the year 2300 (Fox-Kemper et al., 2021; Coulon et al., 2024; Klose et al., 2024; Seroussi et al., 2024). The rate of ice loss is influenced by many processes such as atmospheric and oceanic processes, and ice dynamics, which can lead to an uncertainty in sea level change of up to 1.5 meters in 2300 (Seroussi et al., 2024). Accurately representing these processes in models, along with their associated uncertainties, presents a significant challenge for projecting the ice sheet evolution. To address this, a wide range of parameters in the ice-sheet model must be explored, requiring ensemble simulations to produce robust projections of potential sea-level rise over the coming centuries (Seroussi et al., 2020).

One of the main uncertainties in projecting the evolution of the AIS over the next centuries is the response of the solid Earth to future changes in ice mass (Fox-Kemper et al., 2021). The bedrock experiences uplift due to the loss of ice mass at the surface, a process known as glacial isostatic adjustment (GIA). The bedrock uplift can delay grounding line retreat and thereby stabilize the ice sheet ((Gomez et al., 2015; Whitehouse et al., 2019)). The rate of the bedrock uplift depends on the viscosity of the Earth's mantle, which varies both radially and laterally by several orders of magnitude beneath the AIS (Kaufmann et al., 2005; Ivins et al., 2023), as derived from seismic models (e.g. Lloyd et al., 2019). Therefore, bedrock uplift is influenced not only by the amount of ice mass loss but also by the solid Earth properties of the region where the loss occurs. Models that include the bedrock deformation for a 3D Earth structure project a maximum of 23-40% reduction in sea-level rise over the coming centuries compared with models that assume a rigid Earth (Gomez et al., 2024; van Calcar et al., 2024), and a delay in grounding line retreat in the Amundsen Sea Embayment by up to 130 years (van Calcar et al., 2024). However, it is currently unfeasible to include a 3D GIA model in a large ensemble of sea-level projections that use dynamic ice sheet models due to the long computation time involved (van Calcar et al., 2023). Therefore, projections of AIS evolution by ice-sheet models either omit bedrock uplift or use simplified Earth models (Levermann et al., 2020).

One such simplified model that is commonly coupled to ice-sheet models is the elastic lithosphere, relaxed asthenosphere (ELRA) model (Le Meur and Huybrechts, 1996). ELRA models are computationally cheap, easy to implement in ice sheet models, and can be used in combination with a range of ice models, allowing large ensembles of sea-level projections to be simulated (Bulthuis et al., 2019; Levermann et al., 2020; DeConto et al., 2021; Coulon et al., 2024). Typically, ELRA is used with a uniform relaxation time of 3000 years and a flexural rigidity of 10^{25} kg m^2 s^{-2}, which roughly corresponds to a lithospheric thickness of 100 km (Le Meur and Huybrechts, 1996; Bulthuis et al., 2019; Levermann et al., 2020; DeConto et al., 2021; Coulon et al., 2024). The relaxation time of the Earth's mantle, which is a characteristic time scale that expresses how fast the mantle responds to changes in surface loads, serves as a proxy for mantle viscosity because it also reflects how fast the viscous mantle flows under stress.

Alternatively, some sea-level projections use ice-sheet models coupled with a 1D GIA model. A GIA model includes the bedrock deformation due to changes in ice loading, and can additionally solve the sea level equation to include changes in ocean loading. In this study, we use the term GIA model for a model that computes deformation based on ice loading only. A

heeft verwijderd: ice sheet
heeft verwijderd:
heeft verwijderd: over
heeft verwijderd: next centuries
heeft verwijderd:).
heeft verwijderd: feedbacks,
heeft verwijderd: and interactions with the underlying bedroc
heeft verwijderd:
heeft verwijderd: thousands of
heeft verwijderd:
heeft verwijderd: Antarctic ice sheet
heeft verwijderd: (Konrad
heeft verwijderd: Pollard et al., 2017;
heeft verwijderd: ; Kachuck et al., 2020; Coulon et al., 2021; Book et al., 2022; Gomez et al., 2024; van Calcar et al., 2024).
heeft verwijderd: Antarctic ice sheet
heeft verwijderd: specific
heeft verwijderd: solid Earth feedback
heeft verwijderd: realistic
heeft verwijderd:
heeft verwijderd: realistic Earth structure
heeft verwijderd:
heeft verwijderd: the Antarctic ice sheet
heeft verwijderd:
heeft verwijderd:
heeft verwijderd: .
heeft verwijderd:
heeft verwijderd: the
heeft verwijderd: model
heeft verwijderd: .
heeft verwijderd: Flexural rigidity is the resistance of a body such as the Earth's lithosphere, to bending and is determined, amo other, by its stiffness (the elastic modulus) and its thickness.
heeft verwijderd:
heeft verwijderd:
heeft verwijderd: can include
heeft verwijderd: response

1D GIA model includes an Earth structure where viscosity varies radially and not laterally, equivalent to a self-gravitating viscoelastic Earth (SGVE) model (Le Meur and Huybrechts, 1996). Current existing ice sheet projections that are derived in conjunction with a 1D GIA model use a homogeneous upper mantle viscosity of 10^{21} Pa·s (Gomez et al., 2015; Konrad et al., 2015; Rodehacke et al., 2020; Golledge et al., 2015; Klose et al., 2024). However, using such a viscosity value, or a relaxation time of 3000 years, does not affect sea-level rise projections significantly compared with excluding bedrock deformation entirely, and it overestimates sea-level rise by up to 20% by the year 2500 compared with projections that use GIA models that consider 3D Earth structure, which we refer to as 3D GIA models (van Calcar et al., 2024).

In the Amundsen Sea embayment, mantle viscosity can be as low as 10^{19} Pa·s (Barletta et al., 2018). Incorporating a low-viscosity zone in the upper mantle within a 1D GIA model leads to a significant stabilizing effect on the ice sheet over thousands of years (Pollard et al., 2017). However, the same study showed that different relaxation times for East and West Antarctica did not contribute significantly to the uncertainty in the multi-centennial response of the AIS to climate change. This can be explained by the chosen relaxation times for West Antarctica which were longer than 1000 years, while they might be a lot shorter in this region (Bulthuis et al., 2019). Other research has demonstrated that using a laterally varying relaxation time in ELRA (LVELRA) with a shorter relaxation time under West Antarctica results in a significantly reduced sea level contribution from Antarctica on multicentennial-to-millennial timescales for four different warming scenarios of 5000 years (Coulon et al., 2021). While it has long been possible to determine relaxation time spectra for radially varying viscosity profiles (McConnell, 1965), such calculations have not been performed for profiles with both lateral and radial variations in viscosity. Consequently, the variation in mantle relaxation times across Antarctica remains unknown.

A laterally varying relaxation time can be implemented in a straight-forward way in an ELRA model (Oude Egbrink, 2018; Coulon et al., 2021). However, sea-level projections generated using coupled ELRA-ice-sheet models have not been compared with the output from coupled ice sheet-3D GIA models, leaving it unclear how well different relaxation times and 1D mantle viscosity profiles are able to approximate the deformation simulated by more complex models that include 3D Earth structures. Relatively fast GIA models that incorporate laterally varying viscosity and could, in principle, be coupled to ice sheet models do exist (Nield et al., 2018; Book et al., 2022; Weerdesteijn et al., 2023). However, these are regional, flat-Earth models, which can introduce substantial errors when applied to Antarctic-wide simulations. A computationally efficient Earth model based on fast Fourier transforms has also been developed to approximate lateral variations in mantle viscosity and lithospheric thickness in Earth structure (Swierczek-Jereczek et al., 2024). While containing multiple advantages over ELRA, this model has only been evaluated over a full glacial cycle and not for future projections, and it shows notable discrepancies compared to the 3D GIA model it was benchmarked against. In this study, we therefore focus on assessing the performance of the Earth models already used in ice sheet modelling in current literature.

We use the average sea level contribution from the ice-sheet model IMAU-ICE coupled to a 3D GIA model with two different realizations of 3D Earth structures as a reference, and we use the ice-sheet model coupled to ELRA and a 1D GIA model to answer the following research questions:

heeft verwijderd:
heeft verwijderd: 2019).
heeft verwijderd:
heeft verwijderd: GIA
heeft verwijderd:
heeft verwijderd: using
heeft verwijderd: Antarctic ice sheet
heeft verwijderd: the
heeft verwijderd: model
heeft verwijderd:
heeft verwijderd:
heeft verwijderd: behaviour seen in
heeft verwijderd: structure. We used the ice sheet model IMAU-ICE…
heeft verwijderd: and a GIA
heeft verwijderd: to answer
heeft verwijderd: following research questions:
heeft verwijderd: How well can

1. What is the best parameter choice for a coupled ice sheet – ELRA model using uniform relaxation time to approximate the ice sheet evolution resulting from the reference ?
2. What is the best parameter choice for a coupled ice sheet – ELRA model using laterally varying relaxation time to approximate the ice sheet evolution resulting from the reference ?
3. What is the best parameter choice for a coupled ice sheet – 1D GIA model to approximate the ice sheet evolution resulting from the reference?

To address these questions, 3D GIA simulations are conducted using a global spherical finite element model (van der Wal et al., 2013; van der Wal et al., 2015; Blank et al., 2021, van Calcar et al., 2023) coupled to the ice sheet model IMAU-ICE (Berends et al., 2022; van Calcar et al., 2024). We use constraints from seismic velocity studies to determine the spatially-varying rheological properties of the mantle (Wu et al., 2013). Output from models that employ 3D and 1D Earth structures, and maps of different relaxation times are compared in terms of sea level rise, grounding line position, ice thickness and bedrock uplift. As a result, we recommend values for uniform relaxation times in combination with a flexural rigidity that results in a sea level rise close to the average sea level rise resulting from two 3D Earth structures, one based on a viscosity constraint in the Amundsen Sea Embayment, and one based on a constraint in the Weddell Sea Embayment and Palmer Land in the Antarctic Peninsula. Furthermore, we derive a relation between relaxation time and viscosity and recommend a laterally varying relaxation time map in combination with a flexural rigidity. Last, we recommend a 1D viscosity profile to approximate a 3D viscosity profile.

2 Method

To compare the performance of the ELRA, LVELRA and 1D GIA models with that of a 3D GIA model, we conduct sea level projections using the ice sheet model IMAU-ICE coupled to all three of these Earth models. We compare the AIS evolution over the next 500 years under different warming scenarios and climate models using a variety of Earth structures. We use the projections of two climate models from the sixth phase of the Coupled Model Intercomparison Project (Eyring et al., 2016), namely CESM2-WACCM (hereafter referred to as CESM, Danabasoglu et al., 2020) and IPSL-CM6A-LR (hereafter referred to as IPSL, Lurton et al., 2020), under a low emission scenario (SSP1.2-6) and a high emission scenario (SSP5.8.5) (Coulon et al. (2024); Klose et al., 2024). These two climate models both show warming around the whole West Antarctic Ice Sheet, but forcing magnitudes, and long-term projections of precipitation, atmospheric temperature, and oceanic temperature and salinity differ. In CESM, ocean warming mainly occurs in the Weddell Sea, whereas in IPSL, the warming mainly occurs in the Amundsen Sea. Warming is projected in the Ross Sea for both climate models. The climate models provide ocean temperature, salinity and atmospheric temperature anomalies, and precipitation ratios until the year 2300, which are used to force the ice sheet model. Since there are no climate projections available beyond 2300, the forcing is kept constant between 2300 and 2500. The ocean temperature anomalies are shown in Supplementary Fig. 1 for each climate model and emission scenario.

heeft verwijderd: a coupled ice sheet - GIA model using a Earth structure
heeft verwijderd: How well can
heeft verwijderd: a coupled ice sheet - GIA model using a Earth structure
heeft verwijderd: How well can
heeft verwijderd: with a 1D Earth structure
heeft verwijderd: this model with a 3D Earth structure
heeft verwijderd:
heeft verwijderd:
heeft verwijderd: the
heeft verwijderd:
heeft verwijderd:
heeft verwijderd: land
heeft verwijderd:
heeft verwijderd:
heeft verwijderd: GIA
heeft verwijderd: (van Calcar et al., 2024).
heeft verwijderd: Antarctic ice sheet
heeft verwijderd: An overview of the simulations with differ Earth models is provided in table 1.
heeft verwijderd: the
heeft verwijderd: and the
heeft verwijderd: CESM, where
heeft verwijderd: sea, and
heeft verwijderd: with
heeft verwijderd:
heeft verwijderd: The

The thermomechanically coupled model IMAU-ICE is based on the shallow ice and shallow shelf approximations (Morland, 1985; Bueler & Brown, 2009; Berends et al., 2022). Ice velocities are computed on a 16 km grid resolution. At the grounding line, we applied the flotation condition melt parameterization. The position of the grounding-line can freely evolve from the physics and numerics of the model without explicitly forcing a flux. Basal sliding follows the regularized Coulomb law (Zoet & Iverson, 2020). Basal melt at the ice shelf is computed using the local Favier quadratic method and the surface mass balance is computed using a temperature and radiation parametrization (Favier et al., 2019; Berends et al., 2022). The present-day bedrock and ice surface topography are taken from Bedmachine version 3 (Morlighem et al., 2020). The model does simulate marine ice shelf instabilities, but not marine ice cliff instabilities.

The barystatic sea-level contribution is calculated as the change in ice volume above flotation relative to the initial state. Ice volume above flotation depends on both ice thickness and bedrock elevation, taking into account the bedrock deformation from the different Earth models. The resulting volume change is divided by the global ocean area (taken as $3.611 \cdot 10^{14}$ m^2) and multiplied by the ratio of ice density (taken as 910 kg/m^3) to ocean water density (taken as 1028 kg/m^3).

The ice-sheet model is coupled to an ELRA and a GIA model. The coupling method is discussed in detail in van Calcar et al. (2023) and van Calcar et al. (2024). An overview of the simulations with different Earth models is provided in Tab. 1. The bedrock deformation is computed based on the change in grounded ice thickness above flotation, which is computed by the ice-sheet model. In turn, the bedrock topography in the ice-sheet model is updated by the bedrock deformation provided by the ELRA or GIA model.

Besides the stabilising effect of bedrock deformation on ice-sheet evolution, there is also a sea surface height component, and together these comprise the sea-level feedback. The loss of gravitation from the ice sheet causes a local sea-level drop of up to 8 meters by the year 2500, particularly near regions of major ice loss in the West Antarctic Ice Sheet (van Calcar et al., 2024). However, this 8-meter drop in local sea level is small compared to the effect of bedrock deformation from ice mass changes, which results in up to 150 meters of uplift by 2500. Additionally, gravitational changes due to Earth deformation affect sea level. This additional stabilising feedback from the spatially and temporally varying sea surface height reduces barystatic sea-level projections in 2500 by 5 percent compared to simulations where sea level is fixed at present-day. Previous studies have likewise shown that the deformational component of GIA dominate the sea-level feedback on ice-sheet evolution (Kachuck et al., 2020; Coulon et al., 2021). In all simulations presented in this study, the gravitational effect on sea level is not taken into account and sea level is therefore kept fixed at present-day in both the GIA and ice-sheet models.

Table 1: Different Earth structures used in the coupled ice sheet – Earth models. The 2D relaxation time in the ELRA model is described in detail in section 3. The 1D viscosity profiles correspond to uniform upper mantle viscosities of 10^{21}, 10^{20} and 10^{19} Pa·s,

heeft verwijderd: ice dynamical

heeft verwijderd: 1:

respectively. 1DASE refers to an upper mantle viscosity as suggested by Barletta et al. (2018). All 1D viscosity profiles are shown in Fig. 1. The 3D-stronger and weaker structures are taken from van Calcar et al. (2024).

Model	Input	Earth structures
ELRA	Uniform	- Relaxation time: 3000, 1500, 500, 450, 400, 350, 300, 250 & 200 yr - Lithospheric thickness: ~100 & ~60 km
	2D relaxation time	- Based on 3D-stronger & 3D-weaker - 2 different fits between relaxation time and viscosity - Lithospheric thickness: ~120 & ~60 km
1D GIA	1D profiles	1D21, 1D20, 1D19 & 1DASE
3D GIA	3D rheologies	3D-stronger & 3D-weaker

2.1 1D and 3D GIA models

To compute the Earth's deformation, a global spherical finite element model based on Abaqus software is used (van der Wal et al., 2013; van der Wal et al., 2015; Blank et al., 2021, van Calcar et al., 2023). The model includes material compressibility and excludes the rotational feedback effect and the migration of coastlines caused by changes in sea level, as these are minor effects relative to the effect of change in grounded ice thickness (Milne et al., 1999). This model is used for two purposes: (1) To produce sea-level projections via coupling to the ice-sheet model, and (2) to calculate the relaxation time of the bedrock deformation as a response to schematic ice unloading experiments which are used to derive a relation between relaxation time and viscosity.

In the GIA model, deformation in the upper mantle is assumed to be governed by diffusion and dislocation creep in olivine (Hirth & Kohlstedt, 2003) as in earlier studies (van der Wal et al., 2013; van der Wal et al., 2015; Blank et al., 2021, van Calcar et al., 2023; van Calcar et al., 2024). We do not specify lithospheric thickness, but instead use seismic velocity perturbations to assign appropriate rheological properties in each element between 35 and 670 km depth. At shallower depths, the layer is defined to be purely elastic. At deeper depths, the lower mantle is assumed to be homogenous. The effective viscosity, η_{eff}, is a function of the von Mises stress, q, and hence it is an output of the model rather than a property that is assumed *a priori*:

$$\eta_{\text{eff}} = \frac{1}{3B_{\text{diff}} + 3B_{\text{disl}} q^{n-1}} \quad (1)$$

Here, n is the stress exponent, and B_{diff} and B_{disl} are creep parameters for diffusion and dislocation creep as shown in Eq. 2a and 2b (Hirth and Kohlstedt, 2003).

$$B_{diff} = A_{diff} d^{-3} f_{H_2O}^{1} e^{-\frac{E+PV}{RT(x,y)}} \quad (2a)$$

heeft verwijderd: Weaker
heeft verwijderd: ELRA
heeft verwijderd: 1D GIA
heeft verwijderd: 3D GIA
Met opmaak: Kop 2
Tabel met opmaak
heeft verwijderd: 3D-stronger
heeft verwijderd: (3000, 1500, 500, 400, 300, 200, 50 yr)
heeft verwijderd: 1D21
Samengevoegde cellen
heeft opmaak toegepast: Lettertype: Niet Vet
heeft opmaak toegepast: Lettertype: Niet Vet
Met opmaak: Kop 2
Met opmaak: Lijstalinea, Regelafstand: Meerdere 1,15 rg
Met opsommingstekens + Niveau: 1 + Uitgelijnd op: 0 cm
Inspringen op: 0,63 cm
heeft verwijderd: 2D-stronger
heeft verwijderd: 1D20
Met opmaak: Kop 2
Met opmaak: Lijstalinea, Regelafstand: Meerdere 1,15 rg
Met opsommingstekens + Niveau: 1 + Uitgelijnd op: 0 cm
Inspringen op: 0,63 cm
heeft verwijderd: 2D-weaker
heeft verwijderd: 1D19
Met opmaak: Kop 2
heeft verwijderd: 1D18
Met opmaak: Kop 2
heeft verwijderd: .
heeft verwijderd: realistic
heeft verwijderd:
heeft verwijderd:
heeft verwijderd: B_{diff}
heeft verwijderd: A_{diff}

$$B_{disl} = A_{disl} d^0 f_{H_2O}^{1.2} e^{-\frac{E+PV}{RT(x,y)}} \quad (2b)$$

A is experimentally determined (A_{diff} = 10^6 MPa, A_{disl} = 90 MPa), d is the grain size, f_{H_2O} is the water content, E is the activation energy, which is taken to be $335 \cdot 10^3$ kJ/mol for diffusion creep and $480 \cdot 10^3$ kJ/mol for dislocation creep. P is the depth dependent pressure (Kearey et al., 2009). V is the activation volume, which is taken to be $4 \cdot 10^{-6}$ m^3/mol for diffusion creep and $11 \cdot 10^{-6}$ m^3/mol for dislocation creep. R is the gas constant. A, E and V are different according to the values for wet and dry olivine and are given here for wet olivine. All parameters, except temperature, grain size and water content, are taken from Hirth and Kohlstedt (2003). In this study, melt content is neglected as it has a relatively small influence on viscosity in this formulation (van der Wal et al., 2015). $T(x,y)$ is the spatially varying mantle temperature, which is derived from a high resolution seismic model (Lloyd et al., 2019) in combination with a global seismic model from Becker and Boschi (2002). The mantle temperature variations are determined by converting these global seismic velocity perturbations to temperature perturbations using derivatives from Karato (2008), and then converting these to absolute temperature assuming a standard mantle geotherm (Turcotte and Schubert, 2002).

The upper mantle viscosity can vary greatly depending on the grain size and water content used. To obtain a 3D rheology, two different combinations of grain size and water content are chosen such that the average viscosity values across the Amundsen Sea Embayment and the Weddell Sea Embayment are the same as those constrained by GIA observations (Ivins et al., 2023), resulting in a relatively weaker 3D structure (labelled 3D-weaker) and a relatively stronger 3D Earth structure (labelled 3D-stronger) respectively (van Calcar et al., 2024). The 3D-weaker structure contains a water content of 400 ppm and a grain size of 2.5 mm, and the 3D-stronger structure contains a water content of 200 ppm and a grain size of 4.5 mm. Since the viscosity is constrained by observations, both structures are considered realistic and not just an upper or lower limit. Background stress that contributes to the variable q in Eq. 1 is ignored here. Including background stress from the long-term GIA signal would lower viscosity (Blank et al., 2021), which will be compensated by grain size and water content parameters to still match the viscosity constraints.

For the coupling to the ice model, the GIA model is used with 10 vertical layers (0-35 km, 35-100 km, 100-150 km, 150-300 km, 300-420 km, 420-550 km, 550-670 km, 670-1171 km, and 1171-2890 km, and 2890-6371 km). We label this model as Configuration 1 of the GIA model. Laterally varying B_{diff} and B_{disl} are assigned to each element between 35 and 670 km depth following Eq. 2a and 2b, respectively. The viscosity according to Eq. 1 determines if an element behaves effectively elastically; the lithosphere thickness is not specified explicitly. At shallower depths, the layer is defined to be purely elastic. At deeper depths, the lower mantle is assumed to be homogenous with a viscosity of $5 \cdot 10^{21}$ Pa·s. A high resolution area is defined over Antarctica with a horizontal and vertical grid resolution of 30 km wide and deep between the surface and 670 km depth. The sensitivity test for the effect of resolution over a glacial cycle presented in van Calcar et al. (2023) shows that using a horizontal resolution of 15 km by 15 km instead of 30 km by 30 km decreases the total deformation by 0.01% (2 cm) over 1000 years and increases the computation time of the GIA model by approximately 30%. The uncertainty could be larger for

heeft verwijderd: B_{disl}
heeft verwijderd: A_{disl}
heeft verwijderd: A_{diff}
heeft verwijderd: A_{disl}
heeft verwijderd: ,
heeft verwijderd:),
heeft verwijderd: ,
heeft verwijderd: and $T_{x,y}$ is the spatially variable absolute temperature. …
heeft verwijderd:
heeft verwijderd: T_x
heeft verwijderd:
heeft opmaak toegepast: Niet Superscript/ Subscript
heeft verwijderd: realistic
heeft verwijderd: 2024).
heeft verwijderd: ,
heeft verwijderd: 9
heeft verwijderd: elastic
heeft verwijderd: .
heeft verwijderd: 35 km wide and deep between the surface a 670 km depth.

elastic effects with a smaller spatial wavelength and deformation on shorter timescales. However, the uncertainty is significantly smaller than the uncertainty in adopted Earth structure (Wan et al., 2022; van Calcar et al., 2023). The spatial resolution outside the high-resolution area is 200 km.

Different methods can be used to simulate the response due to 1D Earth structures (Peltier, 1974; Wu, 1998) but here we use the same GIA model to simulate a 1D Earth structure and a 3D Earth structure to avoid introducing differences that arise due to model formulation. The relatively high computation time of the GIA model limits the number of cases we can investigate. Four 1D Earth structures are applied in the GIA model: one commonly used structure with an upper mantle viscosity of 10^{21} Pa·s, two structures with an upper mantle viscosity of 10^{20} and 10^{19} Pa·s, respectively, to represent the average viscosity under West Antarctica, and one with an upper mantle viscosity between $5{\cdot}10^{18}$ and $3{\cdot}10^{19}$ Pa·s that could represent the Amundsen Sea embayment (Barletta et al., 2018). These structures are hereafter referred to as 1D21, 1D20, 1D19 and 1DASE, respectively, and their 1D viscosity variations with depth are shown in Fig. 1.

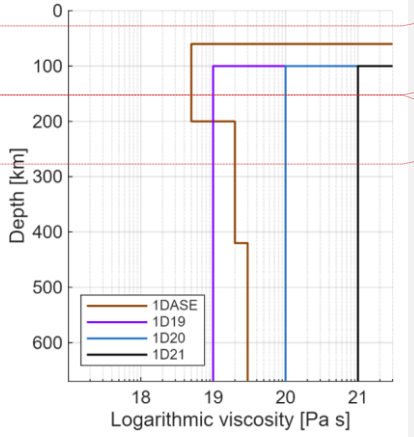

Figure 1: Upper mantle viscosity of the 1D Earth structure profiles.

To derive a relation between relaxation time and viscosity, as discussed in section 3, we used uplift rates from a schematic experiment using a 3D GIA model. In this case, the spatial resolution is 2 degrees at the surface and includes 8 vertical layers following van der Wal et al. (2013) and van der Wal et al. (2015) (0-35 km, 35-70 km, 70-120 km, 120-170 km, 170-230 km, 230-400 km, 400-670 km, and 670-2890 km), which we label as Configuration 2 of the GIA model. This resolution allowed us to run many schematic experiments. We used a global seismic model from Schaeffer & Lebedev (2013) combined with the regional seismic model of Heeszel et al. (2016) derived from Rayleigh wave array analysis over Antarctica to create a global seismic model. Uncertainties in the regional seismic model are used to ensure a smooth transition between values defined by the regional and global seismic models. The mantle temperature is then obtained following the same procedure as described for Configuration 1. The dislocation and diffusion parameters are then computed using the mantle temperature, stresses, and a suite of globally-uniform values for grain size (1, 4, and 10 mm) and water content (0 or 1000 ppm H_2O). Below 400 km, uniform creep parameters are adopted, which yield mantle viscosities of ~10^{21}-10^{23} Pa s. The 3D GIA model is coupled to a code that solves the sea-level equation (Farrell & Clark, 1976) as implemented by Wang and Wu (2006). This configuration is uncoupled from the ice dynamic model and the applied ice loading is further described in section 3.

heeft verwijderd: *<object>*

heeft verwijderd: structures

heeft verwijderd: structures

heeft verwijderd: *<object>*

heeft verwijderd: . Fig 1 shows the

heeft verwijderd: .,

heeft verwijderd: .,

heeft verwijderd: configuration

heeft verwijderd: , and

heeft verwijderd: with variable resolution as ‘configuration

heeft verwijderd: configuration

2.2 ELRA

In ice sheet modelling, the Earth properties are often simplified to the ELRA approximation as described in detail in Le Meur & Huybrechts (1996). In this approach, bedrock deformation is obtained by a convolution of the deformation to a point load with the actual load and is dependent on the flexural rigidity and the relaxation time. The flexural rigidity (D) determines, together with the density of the asthenosphere and the gravity acceleration at the surface, the radius of relative stiffness (L_r) as shown in Eq. 3.

$$L_r = \left(\frac{D}{\rho_a g}\right)^{\frac{1}{4}} \quad (3)$$

First, the equilibrium deflection (w) at a normalized distance (x) from a point load (q) is computed using

$$w(x) = \frac{q{L_r}^2}{2\pi D} \cdot X(x), \quad (4)$$

where X is the zeroth order Kelvin function of x. The normalized distance is defined as the real distance (r) from the point load divided by the radius of relative stiffness. The total deflection at each point is the sum of the deflection at all neighboring points within a distance of six times the radius of relative stiffness.

Second, the bedrock deflection can be computed using

$$\frac{db_{ij}}{dt} = \frac{w_{i,j} - b_{i,j}}{\tau}, \quad (5)$$

where $\frac{db}{dt}$ is the bedrock elevation change over time, b the current bedrock elevation, τ the relaxation time and i, j the grid coordinates.

Besides the commonly used relaxation time of 3000 years and flexural rigidity of 10^{25} N·m, we also applied a relaxation time of 1500, 500, 450, 400, 350, 300, 250, 200 and 50 years in combination with a flexural rigidity of $1.92 \cdot 10^{24}$ N·m. The flexural rigidities roughly correspond to lithospheric thicknesses of 100 km and 60 km, of which the latter is close to the estimated lithospheric thickness of West Antarctica (e.g. An et al. 2015; Pappa et al. 2019). The lithospheric thickness is estimated to be much larger in East Antarctica, but the bedrock deformation in response to ice load change is relatively insensitive to variations in lithospheric thickness compared to the relaxation time (Coulon et al., 2021). The lithospheric thickness can be derived from the definition of flexural rigidity:

$$D = \frac{Eh^3}{12(1-\nu^2)}, \quad (6)$$

with the Young's modulus (E) set to 100 GPa and the Poisson's ratio (ν) set to 0.25. The lithospheric thickness is defined by h.

For the laterally varying ELRA model, we simply made the relaxation time in Eq.5 a function of the 2D grid coordinates, such that τ becomes $\tau(i, j)$. A laterally varying flexural rigidity is also possible to implement but it is more complex (Coulon et al.,

heeft verwijderd:

heeft verwijderd: dependent on a point load,

heeft opmaak toegepast: Lettertype: Cursief

heeft opmaak toegepast: Lettertype: Cursief

heeft verwijderd: $\frac{db(i,j)}{dt}$

heeft verwijderd: $\frac{w(i,j)-b(i,j)}{\tau}$

heeft verwijderd: . This

heeft opmaak toegepast: Lettertype: Cursief

heeft verwijderd:

heeft opmaak toegepast: Lettertype: Cursief

heeft verwijderd: as shown in Eq. 7.¶
$\frac{db(i,j)}{dt} = \frac{w(i,j)-b(i,j)}{\tau(i,j)}$, (7)¶

2021), and the effect on bedrock deformation is limited (Coulon et al, 2021; Zhao et al., 2017; Mitrovica et al., 2011). We therefore used uniform flexural rigidity values of $1.536 \cdot 10^{25}$, $1 \cdot 10^{25}$, $4.5511 \cdot 10^{24}$, and $1.92 \cdot 10^{24}$ N·m, corresponding roughly to lithospheric thicknesses of 120, 100, 80 and 60 km (Eq. 6), in agreement with estimates for lithospheric thickness across West and East Antarctica (Lloyd et al., 2019).

3 Deriving 2D relaxation time maps from 3D viscosity profiles

For a viscous half-space with uniform mantle viscosity, the relaxation time is equal to the Maxwell relaxation time that can be computed directly from the viscosity and shear modulus (e.g. Turcotte and Schubert, 2002). However, in a laterally and radially varying Earth structure, there is no longer a simple relation between Maxwell time and viscosity. In analytic GIA models based on the normal mode method (e.g. Wu & Peltier, 1982), each eigenmode has a characteristic relaxation time, but the complete response is controlled by a weighted combination of modes that depends on the spatial scale of the load and the properties of the lithosphere. This implies that the relaxation time that is induced by a certain change in ice load for a given viscosity profile depends on the size of the ice (un)loading. Thus, a single, uniform relaxation time constant in time cannot be directly derived from a local viscosity.

Here, using the 3D GIA model in Configuration 2, we determine relaxation times empirically by analysing the solid Earth deformation triggered by the removal of schematic surface loads with the aim to derive a relationship between relaxation time and viscosity that can be used for any viscosity map without a priori constraints on where ice loss is exactly taking place. The surface loads are chosen to reflect large and small areas of ice mass change for different regions in West Antarctica. The small area is chosen to cover the main area of mass loss close to the present-day grounding line. The large area is chosen to cover the full basin of the Embayment, or the Peninsula. By applying schematic ice loads in various locations, the resulting empirical relation between mantle viscosity and relaxation time accounts for a wide spectrum of mantle conditions such that the relation is valid over a large viscosity range, including mantle viscosities similar to those found around the grounding line in East Antarctica. The resolution of the 2-degree finite element mesh that is used in this configuration of the 3D GIA model is relatively coarse, and therefore determines the exact shape of each area of loading (Fig. 2a). The uniform thickness of each load is taken to be 500 m to approximate stress changes comparable to those expected in realistic ice loss scenarios. To reduce computational costs, only the wavelength of the ice load is varied, and not the ice thickness, as the normal mode theory shows that wavelength is most influential on relaxation time derived from deformation. Each load is placed on the Earth until equilibrium is reached, and then instantaneously removed.

A total of 40 simulations are conducted, using a grain size of 1, 4 and 10 mm, a water content of 0 and 1000 ppm and a small, medium and large of the region of loading (as shown in Fig. 2a).. For each simulation, the displacement over time for each surface load/Earth model combination is computed. Each simulation contains 20 timesteps, of which the first time step is 15 years, increasing by a factor of 1.5 until the largest time step of 33.3 kyr. From the displacement curve, the uplift rate through time is calculated by time differentiation. The relaxation time is computed as half the time it takes for solid Earth rebound rates to decrease by $1/e^2$ following instantaneous unloading (Table 1 in Supplementary materials). Averaging over two relaxation

heeft verwijderd: Relation between 3D viscosity and
heeft verwijderd: more realistic
heeft verwijderd: sheet and that
heeft verwijderd: .
heeft verwijderd: configuration
heeft verwijderd: . These
heeft verwijderd: , such that the
heeft verwijderd: relationship
heeft verwijderd: the different
heeft verwijderd: beneath the regions where the load changes taking place. The shape of each surface load is controlled by the
heeft verwijderd: (Fig. 2a). The uniform thickness of each lo is taken to be 500 m.
heeft verwijderd: varying the
heeft verwijderd: ,
heeft verwijderd: and
heeft verwijderd: .
heeft verwijderd: for multiple time steps.
heeft verwijderd: Supplemental

times reflects more accurately the fact that viscosities at different depths will control the deformation at different stages of the relaxation. The difference in relaxation time between the large and small region of loading is on average 12% (31 years), with one outlier of 45% (47 years) in the Amundsen Sea Embayment where a large area of ice mass loss (indicated by pink and red in Fig. 2a) leads to a significantly lower relaxation time than a smaller area of ice mass loss (indicated by pink in Fig. 2a). This large difference only occurs for a water content of 1000 ppm and a grainsize of 1 cm.

Typically, depth averaged viscosities are computed by taking the average of the logarithmic viscosity values in a certain layer or area (e.g. Paulson et al., 2005; Whitehouse et al., 2006; Bagge et al., 2021). The filled symbols in Fig. 2b show the characteristic relaxation time of each region plotted against the average mantle viscosity, calculated as the volume-weighted mean viscosity of all elements between 120 and 400 km depth beneath each unloaded region indicated in Fig. 2a. However, the region in the mantle that primarily governs the Earth's response is determined by how strongly the Earth's deformation under the ice load is influenced by viscosity at different depths, which in turn depends on the viscosity profile itself (Peltier, 1976; Wu 2006). The sensitivity to the viscosity profile can be taken into account by computing the vertically averaged viscosities weighted by the local strain rate (Christensen, 1984). Such a procedure would result in average viscosity values that are determined more by low viscosity values in sub-surface Antarctica (because low viscosity regions will experience the highest strain rates). To take that into account, the computed relaxation times are compared to not only the average mantle viscosity value for each region, but also the lowest mantle viscosity derived from the seismic model, which is shown by the open symbols in Fig. 2b. A linear fit through the resulting log-log graph provides a relation between relaxation time in years, τ, and viscosity in Pa·s for the average viscosity (solid line in Fig. 2) and the lower bound viscosity (dashed line in Fig. 2). The linear fit is determined by Eq. 7:

$$\tau = a \cdot 10^{-b} {\eta_{eff}}^{c} \quad (7)$$

where a is 2.3, b is 5, and c is 0.35 in the case when the average viscosity is used, and a is 3.9, b is 2 and c is 0.20 in the case when the lower bound viscosity is used. Both relations will be used to create 2D relaxation time maps to identify which one is best approximating the sea-level rise projections resulting from the coupled 3D GIA – ice-sheet model. When the 2D relaxation time maps are used in an ELRA model, the relaxation time should be smoothly varying because otherwise discontinuities in deformation arise for adjacent points. Either a high-resolution viscosity profile should be used, because this will likely not contain large sharp changes in viscosity, or the relaxation time map should be smoothed, as applied in this study.

heeft verwijderd: log of the

heeft opmaak toegepast: Engels (Verenigd Koninkrijk)

heeft verwijderd: actual

heeft verwijderd: of

heeft verwijderd: predominantly influences

heeft verwijderd: depends on

heeft verwijderd: sensitivity of

heeft opmaak toegepast: Engels (Verenigd Koninkrijk)

heeft opmaak toegepast: Engels (Verenigd Koninkrijk)

heeft opmaak toegepast: Engels (Verenigd Koninkrijk)

heeft opmaak toegepast: Engels (Verenigd Koninkrijk)

heeft opmaak toegepast: Engels (Verenigd Koninkrijk)

heeft verwijderd: Earth to the specific loading

heeft opmaak toegepast: Engels (Verenigd Koninkrijk)

heeft opmaak toegepast: Engels (Verenigd Koninkrijk)

heeft opmaak toegepast: Engels (Verenigd Koninkrijk)

heeft verwijderd: Eq. 8,

heeft verwijderd: Eq. 9,

heeft verwijderd: $\tau = 10^{\log(\eta_{eff})\cdot 0.35 - 4.63}$ (8)¶
$\tau = 10^{\log(\eta_{eff})\cdot 0.20 - 1.41}$ (9)¶

heeft verwijderd:

heeft verwijderd:

heeft verwijderd: .

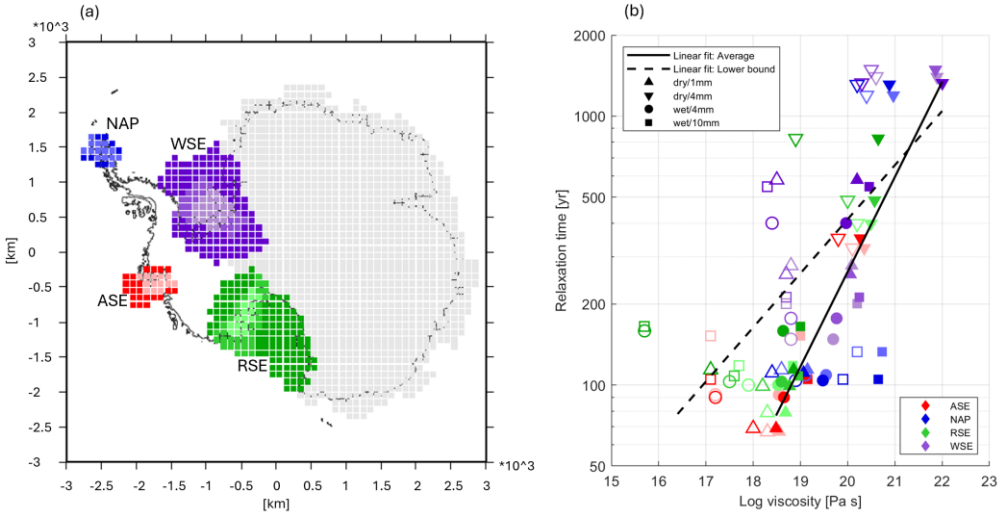

Figure 2: The relationship between mean upper mantle viscosity and relaxation time across West Antarctica. (a) Regions from which ice is instantaneously unloaded in order to determine regional relaxation times. Within each of the four main regions, there is a large and a small version of the region, coloured in dark and light colours respectively. The small region overlaps the large region. NAP refers to Northern Antarctic Peninsula, WSE refers to Weddell Sea Embayment, ASE refers to Amundsen Sea Embayment, and RSE refers to Ross Sea Embayment. (b) Log-log plot of relaxation time against mean upper mantle viscosity and the lower bound viscosity. The colours are identical to (a). The symbols reflect the parameters in the 3D GIA model used in each experiment (see Supplementary Table 1). The filled symbols reflect the average viscosity and the open symbols reflect the lower bound viscosity.

Using our empirically derived relationships between viscosity and relaxation time (Eq. 7), we derive laterally variable relaxation time maps based on the 3D-weaker and 3D-stronger Earth models described in Section 2.1. η_{eff} is taken to be the viscosity of the 3D Earth structure vertically averaged between 120 and 400 km depth (Fig. 3a,d). For ice thickness changes over a timescale of centuries, the highest sensitivity will be in this relatively shallow layer (Barletta et al., 2018). This results in two relaxation time maps based on the 3D-weaker rheology, hereafter referred to as 2D-weaker Average and 2D-weaker Lower bound (Fig. 3 b-c), and two relaxation time maps based on the 3D-stronger rheology, hereafter referred to as 2D-stronger Average and 2D-stronger Lower bound (Fig. 3 e-f). Finally, the minimum relaxation time is set to 67 years, equal to the minimum relaxation time found in the experiments used to derive Eq. 7.

heeft verwijderd: Extended Data

heeft verwijderd: 8, 9

heeft verwijderd: section

heeft verwijderd:

heeft verwijderd: the

heeft verwijderd: in the projections

heeft verwijderd: the ice sheet evolution by the ice sheet mod

heeft verwijderd: 8 and Eq. 9

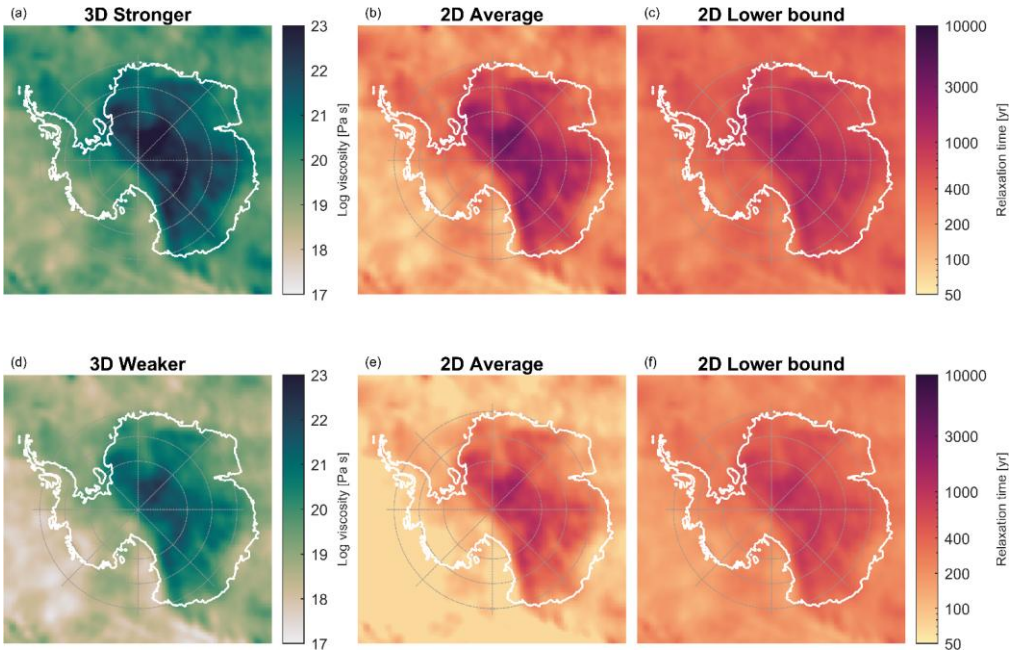

Figure 3: Panels a and d show the vertically averaged mantle viscosity between 120 and 400 km depth based on van Calcar et al. (2024). Panels b and e show the relaxation time maps computed using Eq. 7 with the parameters for the average viscosity fit, and 3D-stronger and 3D-weaker, respectively. Panels c and f show the relaxation time maps computed using Eq. 7 with the parameters for the lower bound viscosity fit, and 3D-stronger and 3D-weaker, respectively.

4 Projections using different approaches to bedrock deformation

Sea-level rise over the next 500 years is projected using two different climate models, each under a high and a low emissions scenario. Projections using simple models that adopt a uniform relaxation time, a laterally variable relaxation time, and a 1D Earth structure are compared to the average sea-level rise obtained using the 3D-weaker and 3D-stronger Earth structures within the GIA model in Configuration 1. The average barystatic sea-level rise computed by the ice-sheet model using the two different 3D Earth structures is referred to as 3D-Average.

We found a significantly higher sea-level contribution in our simulations compared to other studies using the same forcing, which likely stems from differences in key model components, particularly the initialisation, the basal melt scheme, and the melt parametrization at the grounding line (Coulon et al., 2024; Klose et al., 2024), which can lead to large variations in ice sheet evolution and corresponding sea-level rise (Seroussi et al., 2024). Other climate models provide significantly different thermal forcings in terms of magnitude and spatial distribution, which might not be captured by the two climate models used

heeft verwijderd: 8
heeft verwijderd: 9
heeft opmaak toegepast: Tekstkleur: Auto
heeft verwijderd: response
heeft opmaak toegepast: Engels (Verenigd Koninkrijk)
Met opmaak: Geen opsommingstekens of nummering
heeft verwijderd: The sea
heeft verwijderd: for the coming 500 years
heeft verwijderd: for
heeft verwijderd: The sea level rise projected
heeft verwijderd: is
heeft verwijderd:
heeft verwijderd: projected when
heeft verwijderd: configuration
heeft verwijderd:
heeft verwijderd:
heeft verwijderd:

in this study. However, the goal of the present study is to isolate and quantify the relative impact of different Earth structures on Antarctic ice sheet evolution, rather than sampling the full parameter space of IMAU-ICE or to conduct a full intercomparison of model sensitivities. The evolution of the Antarctic ice sheet and the effect of including 3D GIA are discussed in van Calcar et al. (2024).

4.1 ELRA model with uniform relaxation time

For all scenarios and climate models, retreat and thinning of the ice sheet occurs in the West Antarctic Ice Sheet and Wilkes Basin. The bedrock deformation depends indirectly on the climate model because varying ocean warming causes ice retreat in different regions, and the mantle viscosity differs in each region. The bedrock deformation depends on the emission scenario as well, since a larger region of ice mass loss will trigger deformation deeper in the mantle where viscosity, and hence relaxation times, will be different to values at shallower depths (Peltier, 1976). The sea-level rise resulting from the coupled ice sheet – GIA model using a 3D Earth structure therefore differs from a uniform relaxation time, and this difference in turn varies for different emission scenarios and climate models.

To assess the performance of ELRA with a uniform relaxation time, the resulting sea-level rise is compared to the sea-level rise averaged from the output of the two models that employ 3D Earth structures (3D-Average). The widely used uniform relaxation time of 3000 years (hereafter referred to as ELRA3000) overestimates the contribution from the AIS to sea-level rise by 0.44-0.70 m (8-20%) in 2500 compared to the 3D-Average value, with the precise value depending on the emission scenario and the applied climate model (Fig. 4b,c,e,f). First, differences occur because the ELRA model approximates bedrock adjustment as a local viscoelastic response with a single relaxation timescale, while GIA models resolve the full, gravitationally self-consistent, depth-dependent viscoelastic deformation of a layered Earth. Second, differences occur due to the chosen Earth structure in the models. ELRA3000 overestimates sea-level rise because this relaxation time is much longer than the relaxation time associated with the low viscosity values found in the 3D Earth structures (Fig. 3), especially when retreat occurs in the Amundsen Sea Embayment (as predicted by climate model IPSL) where the mantle viscosity is relatively low. We therefore search for a better choice of relaxation time, as formulated in research question 1: How well can a uniform relaxation time approximate the ice sheet evolution resulting from 3D Earth structures?

For SSP2.6-IPSL, the difference in sea-level rise between using a relaxation time of 300 yr (hereafter referred to as ELRA300) and 3D-stronger is negligible until 2400, but increases afterwards, reaching a maximum of 17 cm in 2500 (Fig. 4c), which is 5% of the total of 3.6 m of sea-level rise using 3D-stronger (Fig. 4a). The ice is approximately 50 meter thicker within the Amundsen Sea Embayment using ELRA300 (Fig. 5a) due to faster uplift in this region compared to 3D-stronger. On timescales of 400 years and longer, it is not only the local low viscosity, but also the surrounding higher viscosities, which impact bedrock deformation in the 3D model. The rate of uplift predicted by the 3D GIA model therefore slows down on these longer timescales whereas the relaxation time in ELRA is constant over time and corresponds only to the low viscosities of the 3D model. As a consequence, the amount of bedrock uplift is about 75 m greater in ELRA300 than 3D-stronger between 2400 and 2500. The impact of the difference in bedrock elevation on ice mass loss and grounding line position is negligible. Contrary to this, the

heeft verwijderd: A

Met opmaak: Inspringing: Links: 0 cm, Verkeerd-om: 0, cm

heeft verwijderd: The

heeft verwijderd: response is dependent

heeft verwijderd: of ocean warming cause different regions ice retreat

heeft verwijderd: response

heeft verwijderd:

heeft verwijderd: the

heeft verwijderd: model

heeft verwijderd:

heeft verwijderd:

heeft verwijderd:

heeft verwijderd: ELRA3000 overestimates sea level

heeft verwijderd: figure

heeft verwijderd: Out of the relaxation times investigated, we find that 300 years yields a reasonable approximation for the 3D results until year 2400, in combination with a flexural rigidity corresponding to 100 km lithospheric thickness (Fig. 4). For long simulations, a 500 year relaxation time can be recommended. Wh smaller lithospheric thickness of 60 km is applied, a longer relaxa should be considered (Supplemental Fig. 1). Since the combinatio a higher flexural rigidity and shorter relaxation time yields a simi result to the combination of a lower flexural rigidity and somewh higher relaxation time we only discuss the results for a flexural rigidity corresponding to a 100 km thick lithosphere in the follow For the low emission scenario and by using the climate model IPS the difference in sea

heeft verwijderd:

heeft verwijderd: the

heeft verwijderd: model

viscosity of 3D-weaker is much lower and the uplift predicted by ELRA300 is too slow compared to 3D-weaker over the full simulation time. The bedrock elevation of ELRA300 is tens of meters lower than 3D-weaker in 2300, causing faster retreat to be predicted by ELRA300 until 2500. The grounding line is similar between different Earth models for most of the AIS because bedrock deformation only has an effect in regions where there is mass loss, which in this case is mainly in the Amundsen Sea. In 2500, the grounding line has retreated about 150 km more in this area in ELRA300 compared with 3D-weaker (Fig. 5).

For the high emission scenario, ELRA300 underestimates sea level rise by 0.4 m (6%) in 2500 compared with 3D-Average (Fig. 4a). When there is a larger region of ice mass loss, as is the case in the high emission scenario compared with the low emission scenario, the bedrock deformation is more sensitive to the rheology of deeper parts of the mantle, where the viscosity can be up to 3 orders of magnitude greater than at shallower depths. This causes the same effect as in the low emission scenario – a slowdown of the uplift projected by the 3D model on longer timescales – but the effect is even stronger. The relaxation time of ELRA300 is therefore too short compared to 3D-stronger and 3D-weaker on the long-term, leading to faster uplift and a higher bedrock elevation by 150 m in 2500 (Supplementary Fig. 2). However, around 2300, uplift in the 3D model has not slowed down much and is faster than the uplift of ELRA300. Therefore, at this moment in time, the ice is about 750 meters thicker in 3D-weaker compared with ELRA300 and the grounding line has retreated about 100 km less in the Amundsen Sea Embayment (Supplementary Fig. 3). The slowdown of bedrock uplift is less strong when retreat is concentrated in the Weddell Sea Embayment (using climate model CESM) due to less vertical variation in mantle viscosity in this region (Fig. 4e,f and Supplementary Fig. 4).

The optimal choice of relaxation time is defined as the ELRA simulation with the smallest root mean square error (RMSE) compared to the 3D Average over the full time series, for both climate models and both emission scenarios. The RMSE is shown in supplementary Tab. 1 for each simulation. We find 300 years, with an uncertainty range of 25 years, as approximating closest to the 3D results, in combination with a flexural rigidity corresponding to 100 km lithospheric thickness (Fig. 4). The combination of a higher flexural rigidity and shorter relaxation time yields a similar result to the combination of a lower flexural rigidity and somewhat higher relaxation time and decreasing the lithospheric thickness does therefore not improve the fit of ELRA to the 3D Average (Supplementary Fig. 5).

heeft verwijderd:

heeft verwijderd: response

heeft verwijderd: Supplemental

heeft verwijderd: Supplemental

heeft verwijderd: 4e,f). To conclude, a relaxation time of 300 years fits best until 2400, but a relaxation time of 500 years shoul chosen for longer simulations because of the increasing deviation ELRA300 from 3D-Average over time.

heeft verwijderd: ¶

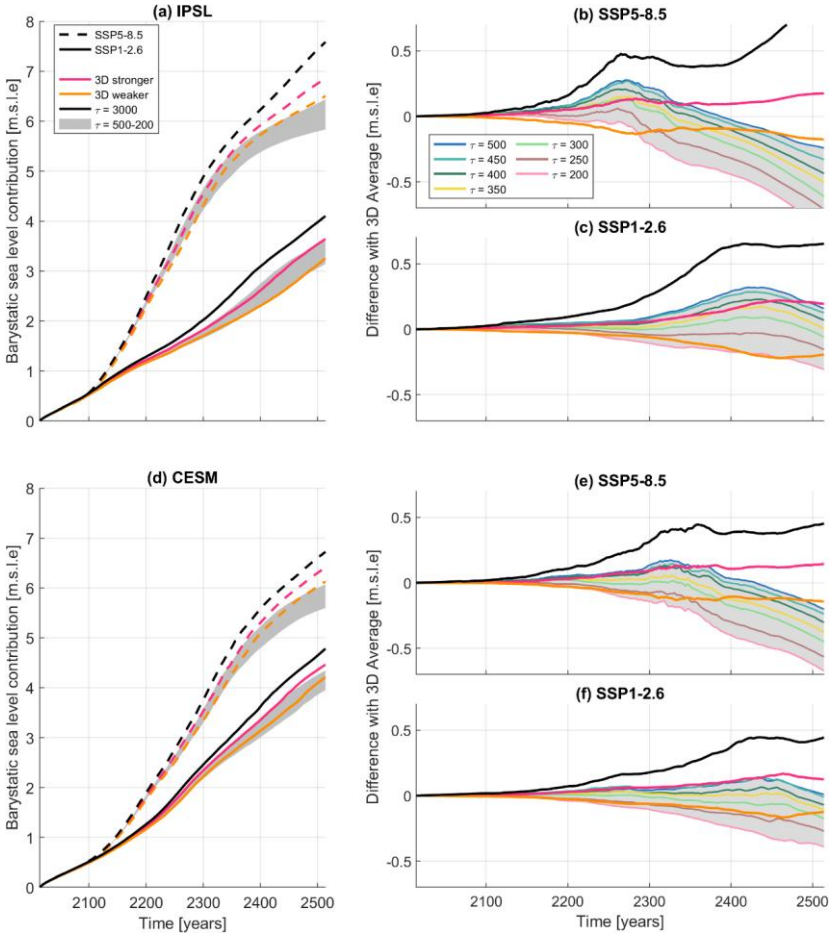

Figure 4. The AIS contribution to barystatic sea level rise using the 3D GIA model and ELRA for a high and a low emission scenario and two different climate models, IPSL-CM6A-LR (panel a) and CESM2-WACCM (panel d). Two different Earth structures are applied in the 3D GIA model, a stronger Earth structure and a weaker Earth structure. The relaxation time of ELRA is varied between 200 and 500 years, and a reference run of 3000 years is used. The flexural rigidity of 10^{25} N·m roughly corresponds to a lithospheric thickness of 100 km. Panels b, c, e, and f show the difference in barystatic sea level contribution between ELRA with different relaxation times and the average sea level contribution of the two 3D GIA simulations.

heeft verwijderd: Antarctic ice sheet
heeft verwijderd:
heeft verwijderd: the
heeft verwijderd: model
heeft verwijderd: the
heeft verwijderd: model
heeft verwijderd: km·m² /s²
heeft opmaak toegepast: Engels (Verenigd Koninkrijk)
heeft verwijderd: the
heeft verwijderd: model

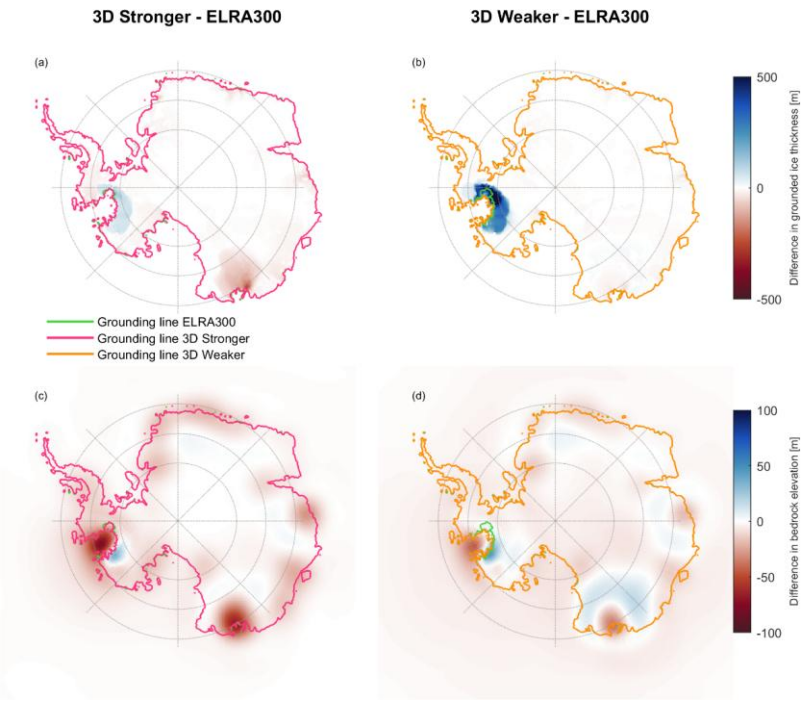

Figure 5: Difference in grounded ice thickness above flotation (panel a and b) and bedrock elevation (panel c and d) in 2500 between ELRA with a relaxation time of 300 years (referred to as ELRA300) and the two 3D Earth structures. Panels a and c correspond to 3D-stronger and panels b and d to 3D-weaker. The climate model IPSL is applied for the low emission scenario SSP1-2.6.

heeft verwijderd: the

heeft verwijderd: model

4.2 ELRA model with 2D laterally variable relaxation time

heeft verwijderd: A

Previous studies presenting the AIS contribution to sea-level rise have shown that a laterally varying Earth structure is needed to accurately simulate AIS evolution (Gomez et al., 2024; van Calcar et al., 2024). As these 3D GIA simulations are very costly, they prohibit large ensemble simulations. We therefore assess the performance of a 2D relaxation time, which is straight forward to implement in an ELRA model, to answer research question 2: How well can a laterally varying relaxation time approximate the ice sheet evolution resulting from 3D Earth structures?

We combined 4 different laterally varying relaxation time maps with different uniform flexural rigidities to investigate how well the computationally efficient ELRA model can replicate the results of the 3D models. As there is no *a priori* reason to select the average or lower bound viscosity equations, or a particular flexural rigidity, we investigate which of the resulting

ice sheet evolutions using the 2D maps correspond best to ice sheet evolution using the 3D-Average, and whether the improvement is significant compared to the performance of ELRA300. The different relaxation time maps, in combination with different lithospheric thicknesses, result in a large range of sea-level rise projections (Fig. 6).

The 2D-stronger map, when combined with a flexural rigidity that corresponds to a lithospheric thickness of 120 km and derived from the average viscosity (Eq. 7), has the smallest RMSE compared to the 3D average, considering both climate models and emission scenarios (Supplementary Tab. 2), and will be considered in the following. For the high emission scenario, the sea-level rise is about 30-40 cm closer to 3D-Average at 2500 using 2D-stronger compared to using ELRA300 (Fig. 6a-b). The advantage of using 2D-stronger over ELRA300 is particularly significant in the Amundsen Sea Embayment projections for scenarios longer than 400 years because the difference between 3D-Average and ELRA300 increases strongly after 2300, whereas the difference between 2D-stronger and 3D-Average is constant over time (Fig. 6a).

On the one hand, the bedrock uplift in the Amundsen Sea Embayment is overestimated by about 250 meters by 2500 when using 2D-stronger compared with using the 3D GIA model in SSP8.5-IPSL (Supplementary Fig. 6). However, this uplift occurs mainly in the last 100 years. Furthermore, the effect on grounding line retreat is small because the grounding line is already retreating rapidly and the West Antarctic Ice Sheet in our simulation is in a phase of collapse. For another ice sheet simulation with different melt approximation or melt parametrization, the sensitivity to a similar uplift might be relatively larger. On the other hand, the uplift is underestimated by up to 60 meters using 2D-stronger compared to using the 3D GIA model in Wilkes basin in East Antarctica. The relaxation time in this area in 2D-stronger is too long to sustain the fast uplift of the 3D GIA model, and the ice mass loss is relatively sensitive to bedrock uplift.

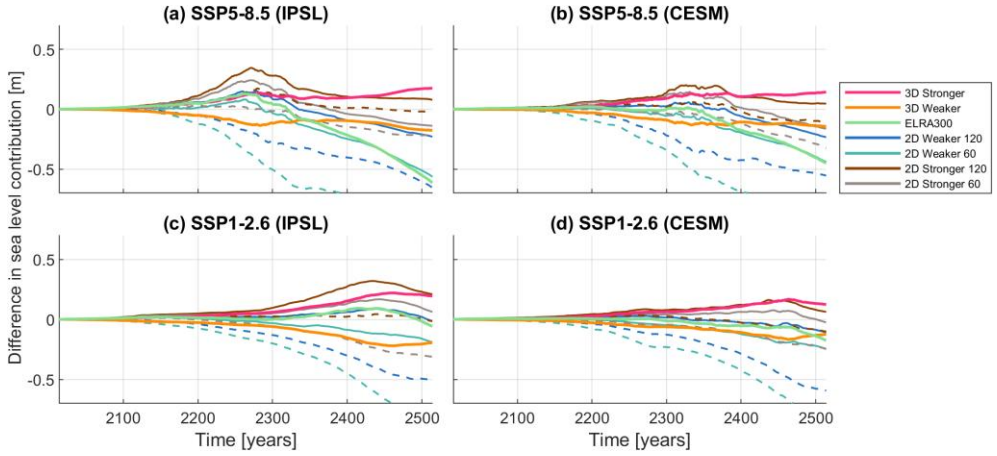

Figure 6: The difference in AIS contribution to barystatic sea-level rise between the average sea level contribution of the two 3D GIA simulations and the contribution using different 2D relaxation time maps. Results are shown for a high and a low emission

heeft verwijderd:
heeft verwijderd: .
heeft verwijderd: 8), produces results which are closest
heeft verwijderd: -Average when
heeft verwijderd: emissions scenarios and
heeft verwijderd: (Fig. 8)
heeft verwijderd:
heeft verwijderd: great
heeft verwijderd: (IPSL)
heeft verwijderd: 6a). In the high emission scenario driven b the IPSL climate model, the bedrock in the Amundsen Sea Embayment uplifted about 250 meters more by 2500 when using stronger compared with using the 3D GIA model (Supplemental 4). However, this uplift occurs mainly in the last 100 years and th effect on grounding line retreat is small due to the fact that the grounding line is already retreating rapidly and the West Antarcti sheet is in a phase of collapse.
Met opmaak: Uitvullen, Regelafstand: 1,5 regel
heeft verwijderd: Antarctic ice sheet
heeft verwijderd:

scenario and two different climate models, IPSL-CM6A-LR and CESM2-WACCM. The dashed lines refer to the relaxation time calculated from the average viscosity and the solid lines refer to relaxation times calculated from the lower bound viscosity (Eq. 7 with corresponding parameters). The numbers 120 and 60 in the legend refer to the lithospheric thickness.

4.3 1D GIA

Some ice sheet models are coupled with a 1D GIA model to conduct projections (Golledge et al., 2015; Gomez et al., 2015; Konrad et al., 2015; Kachuck et al., 2020; Rodehacke et al., 2020; Klose et al., 2024). The 1D GIA model is more realistic than ELRA because it takes into account the radial depth variation of viscosity, which implies a variable relaxation time as the size of the load determines which part of the radial viscosity profile controls the response. As 1D GIA models can also be considered intermediate in terms of computation time compared to ELRA and 3D GIA, we study whether 1D Earth structures offer an improved accuracy compared to ELRA models to answer research question 3: How well can a 1D Earth structure approximate the ice sheet evolution resulting from 3D Earth structures?

A widely used mantle viscosity for a 1D GIA model is 10^{21} Pa·s (hereafter referred to as 1D21) (Gomez et al., 2015; Konrad et al., 2015; Rodehacke et al., 2020; Golledge et al., 2019). Figure 7 shows that 1D21 overestimates the Antarctic sea level contribution by 0.4-0.6 m (6-17%), depending on the emission scenario and climate model, because the structure is too stiff in West Antarctica compared to the 3D structures. The viscosity profiles 1DASE and 1D19 produce results similar to each other and to the 3D-Average model for the low emission scenario but, like ELRA300, they still underestimate the sea level contribution by 0.3 m (4%) in 2500 for the high emission scenario. The viscosity profile 1D19 has the smallest RMSE compared to the 3D Average (Supplementary Tab. 3).

The largest improvement of 1D19 compared to ELRA300 and 2D-stronger is in the bedrock uplift. The bedrock elevation of 1D19 in 2500 differs by a maximum of 80 meters from the results of the 3D GIA modelling in the high emission scenario, which is significantly smaller than the difference of 250 m when 2D-stronger is compared with the 3D GIA model output (Supplementary Fig. 7). This improved agreement is likely explained by the more complete representation of Earth rheology in the 1D GIA model compared to the ELRA approach. While ELRA prescribes a simplified elastic lithosphere and a purely local, exponential relaxation toward isostatic equilibrium, the 1D model captures the full viscoelastic response of the Earth, including both elastic and time-dependent viscous deformation. Although it does not account for lateral variations in Earth structure, the 1D model with low viscosity still resolves the mantle's flow in response to loading, bringing it closer to the behavior captured in 3D GIA models. To replicate not only the sea level contribution from 3D-Average, but also the geometry of the bed, it can therefore be recommended to use a 1D GIA model with an upper mantle viscosity of 10^{19} Pa·s instead of ELRA with a uniform relaxation time of 300 years or the 2D-stronger relaxation time map. Especially for long-term projections under a high emission scenario, the 1D GIA model is preferred over an ELRA model with a uniform relaxation time. However, considering both scenarios and climate models, the 2D-stronger relaxation time map contains the smallest total RMSE over both scenarios and climate models of only 0.17 m compared to a total RMSE of 0.25 m or 0.35 m for 1D19 and ELRA300, respectively (Supplementary Tab. 1, 2 and 3).

heeft verwijderd: (Eq. 8)
heeft verwijderd: 9
heeft verwijderd:
heeft verwijderd: ; Whitehouse et al., 2019
heeft verwijderd:).
heeft verwijderd: the
heeft verwijderd: model
heeft verwijderd: 55
heeft verwijderd: ,
heeft verwijderd: 35
heeft verwijderd: Supplemental Fig. 5).
heeft verwijderd: the
heeft verwijderd: model
heeft verwijderd: .
heeft opmaak toegepast: Lettertype: Niet Vet, Tekstkleu Auto, Engels (Verenigde Staten)

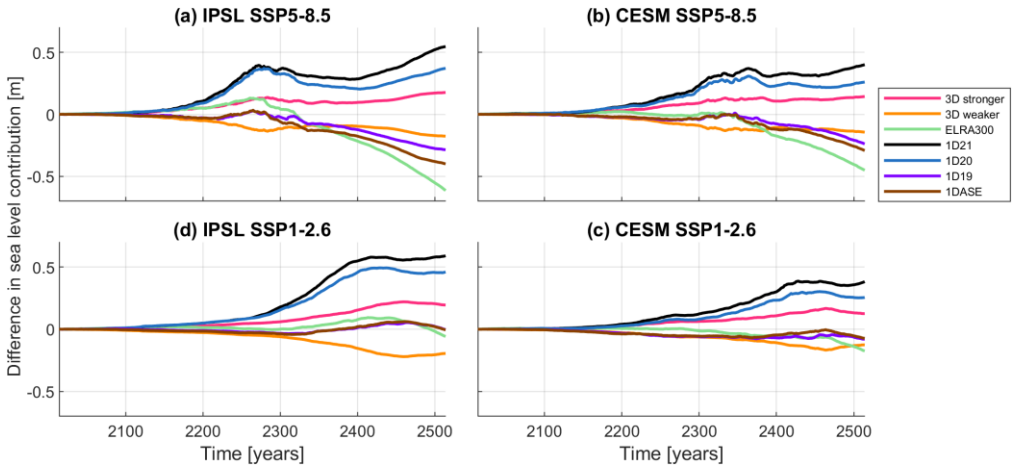

Figure 7: The difference in AIS contribution to barystatic sea level rise between the average sea level contribution of the two 3D GIA simulations and the contribution using different 1D Earth structures. Results are shown for a high and a low emission scenario and two different climate models, IPSL-CM6A-LR and CESM2-WACCM. Note that the 1D19 and 1DASE mostly overlap for IPSL SSP1-2.6.

5 Conclusions and outlook

Using forcing from two climate models under low and high emission scenarios, we investigated the accuracy of common implementations of bedrock displacement in an ice-sheet model by comparison with a coupled ice sheet-3D GIA model. The ELRA model with a commonly used uniform relaxation time of 3000 years combined with a uniform flexural rigidity overestimates sea level rise by up to 0.7 m (20%) compared with the average barystatic sea level rise predicted using a model that includes 3D Earth structures. A 1D GIA model with an upper mantle viscosity of 10^{21} Pa·s overestimates sea level rise by up to 0.6 m (17%). To replicate the sea level rise of the average of the 3D GIA models (3D Average) better, a relaxation time or mantle viscosity corresponding to the area of ice mass loss should be chosen. We investigated the degree to which different bedrock models, Earth structures and parametrisations can replicate the bedrock uplift predicted by models that include 3D Earth structures.

Research question 1 was: How well can a uniform relaxation time approximate the ice sheet evolution resulting from 3D Earth structures? We recommend to use a uniform relaxation time of 275-325 years with a lithospheric thickness of 100 km to replicate the sea level rise predicted by a model that includes 3D Earth structure. Using this relaxation time results in a sea level rise that differs from 3D-Average by only 0.03-0.4 m (0.8-6%), dependent on the emission scenario and the climate model. Note that using this relaxation time does lead to an increasing underestimation of sea level rise from 2400 onwards due to the evolving location and area of ice mass loss which leads to deformation in different regions and influenced by different

heeft verwijderd: Antarctic ice sheet
heeft verwijderd:
heeft verwijderd: .
heeft opmaak toegepast: Tekstkleur: Auto
heeft opmaak toegepast: Tekstkleur: Auto
heeft verwijderd: We
heeft verwijderd: adjustment within
heeft verwijderd: against ice model projections
heeft verwijderd: to a
heeft verwijderd: with 3D variations in viscosity, for differe emission scenarios and climate models
heeft verwijderd:
heeft verwijderd: 70
heeft verwijderd:
heeft verwijderd:
heeft verwijderd: 60
heeft verwijderd:
heeft verwijderd: 300
heeft verwijderd:
heeft verwijderd:
heeft verwijderd: 05
heeft verwijderd: ,
heeft verwijderd:
heeft verwijderd: . Therefore, for simulations longer than 40 years, a relaxation time
heeft verwijderd: 500 years is recommended.

depths of the Earth's mantle. Even though the sea level rise can be similar between ELRA300 and 3D-Average, the ice thickness can locally differ by up to 750 meters, the grounding position may differ by 100 km, and the bedrock elevation may differ by 150 meters between ELRA300 and the different 3D Earth structures. It is therefore recommended to vary the uniform relaxation time between 300 and 500 years to approximate the uncertainty from the 3D Earth structure.

The reduction in sea level rise when using the optimal choice of uniform relaxation time compared to rigid Earth is independent of the total sea level rise in 2500, which means that using the optimal relaxation time causes a larger relative reduction in sea level change when the total sea level rise is lower, for example, in projections from other ice sheet models less sensitive to climate forcing. On millennial timescales, significant ice mass loss might occur in the East Antarctic Ice Sheet (Coulon et al., 2024). While low mantle viscosities of $5 \cdot 10^{18}$ Pa·s might exist in some regions around the present-day grounding line, the viscosity increases up to 6 orders of magnitude inland (Fig. 3a,d). If the majority of the sea level contribution would originate from the East Antarctic Ice Sheet, a larger relaxation time might be necessary.

A spatially varying relaxation time can easily be included in ELRA by directly using a 2D array instead of a single value. We derived an empirical relation between upper mantle viscosity and relaxation time and computed 2D maps of relaxation times to answer research question 2: How well can a laterally varying relaxation time approximate the ice sheet evolution resulting from 3D Earth structures? Applying the 2D-stronger map, derived using the relation between average viscosity for a strong 3D rheology and relaxation time, and a lithospheric thickness of 120 km, results in a sea level rise projection that differs from the 3D-Average value by only 10 cm in 2500. This difference doesn't increase on the long term in contrast to ELRA and it can thus be recommended to use ELRA with spatially varying relaxation time for long term simulations. Still, the bedrock elevation in 2D-stronger is hundreds of meters too high by 2500 compared to the 3D model under a high emission scenario. In this study, we focused on including lateral variations in the ELRA model since this model is already used in sea level projections by ice-sheet models. However, we emphasize the potential of other relatively fast Earth models including lateral variations, such as FastIsostasy (Swierczek-Jereczek et al., 2024) and regional GIA models (Nield et al., 2018; Book et al., 2022; Weerdesteijn et al., 2023).

For models that are able to use a 1D GIA model, we answer research question 3: How well can a 1D Earth structure approximate the ice sheet evolution resulting from 3D Earth structures? The use of an upper mantle viscosity of 10^{19} Pa·s results in sea level rise projections that only differ from 3D-Average by a maximum of 0.3 m. The bedrock elevation in 1D19 differs from 3D-Average by a maximum of 80 meters, thus this model provides the closest resemblance to the 3D Earth structures in terms of geometry, better than the ELRA and LVELRA models. However, the improvement should be traded off against a large increase in computation time. Our recommended values for the relaxation time and 1D viscosity will provide a better approximation of sea level rise than the currently used standard values but should be taken as guidelines and not as the true relaxation time or viscosity of the Earth's mantle. The simplified Earth models are all compared to the same coupled ice sheet - 3D GIA model and this model did not include the effect of a local sea level drop on ice sheet retreat. Including the feedback of the sea level drop on the ice sheet dynamics reduces the sea level rise by 5% compared to using a fixed sea level (van Calcar et al., 2024). Furthermore, using the suggested upper mantle viscosity would lead to an overestimation of the response to

heeft verwijderd:

heeft verwijderd: With a small change in the ELRA model, a spatially varying relaxation time can be included.

heeft verwijderd:

heeft verwijderd: the

heeft verwijderd: model

heeft verwijderd:

heeft verwijderd:

heeft verwijderd:

changes in global ocean loading and to changes in ice loading in East Antarctica over millennial timescales. Finally, different coupled ice sheet-3D GIA models could lead to different projections of sea level contribution, which might lead to somewhat different recommended values for relaxation time and 1D viscosity.

The laterally varying relaxation time is dependent on the 3D viscosity structure so different 2D relaxation time maps could be produced using the provided relation between relaxation time and viscosity. This allows other modellers to create their own relaxation time maps based on their preferred 3D viscosity profiles, for example based on different seismic models, a different time period such as the deglaciation since the last glacial maximum, or for other regions such as Greenland.

heeft verwijderd: . If other regions and time periods are studi these maps could be derived

Code and data availability

The supplementary data, i.e. Table 1 and the laterally varying relaxation time maps, are publicly available with DOI 10.4121/a7215d4c-767f-49f1-a8bb-da40d0d2b01d. The data produced for this publication is available via DOI 10.4121/b5548aaa-4c05-45f7-b0ce-775b83f13e5d. The source code of IMAU-ICE is included in this DOI and can be found on Github: https://github.com/IMAU-paleo/IMAU-ICE. The GIA model code and coupling script has been made publicly available by van Calcar et al. (2023) with DOI 10.4121/19765816.v2.

heeft verwijderd: supplemental

heeft verwijderd: doi

heeft verwijderd: doi

heeft verwijderd: doi

heeft verwijderd: doi

Author contributions

The conceptualisation was done by CvC, WvdW and RvdW. CvC, PW, and WvdW conducted model development and the experiments, and performed the data analysis with input from RvdW. All authors contributed to the writing of the manuscript.

Ethics declarations

There are no competing interests.

Acknowledgements

The authors would like to thank Ann Kristin Klose and Violaine Coulon for preparing and providing the forcing data of the climate models. We thank Matt King, Terry Wilson and Doug Wiens for discussions regarding the computation of relaxation times, and Dirk Oude Egbrink for his master thesis work which provided the first insights into the effect of a laterally varying relaxation time. We thank the reviewers for their thorough and constructive feedback, which has significantly contributed to improving the clarity of the manuscript. Work for this publication was performed in the framework of PROTECT, which received funding from the European Union's Horizon 2020 Research and Innovation Programme under grant agreement No 869304. This is PROTECT publication number xxx (defined upon acceptance). The study was also supported by the project

3D Earth funded by ESA as a Support to Science Element (STSE), and by the UK Natural Environment Research Council as an Independent Research Fellowship (NE/K009958/1).

Additional information

Correspondence and requests for materials should be addressed to Caroline van Calcar (c.j.vancalcar@tudelft.nl).

heeft verwijderd: (c.j.vancalcar@uu.nl).

References

An, M., D. A. Wiens, Y. Zhao, M. Feng, A. Nyblade, M. Kanao, Y. Li, A. Maggi, and J.-J. Lévêque: Temperature, lithosphere-asthenosphere boundary, and heat flux beneath the Antarctic Plate inferred from seismic velocities, *J. Geophys. Res. Solid Earth*, 120, 8720–8742, doi:10.1002/2015JB011917, 2015.

Bagge, M., Klemann, V., Steinberger, B., Latinović, M., and Thomas, M.: Glacial-isostatic adjustment models using geodynamically constrained 3D Earth structures, Geochem. Geophys. Geosyst., 22(11), e2021GC009853, https://doi.org/10.1029/2021GC009853, 2021.

Barletta, V.R., Bevis, M., Smith, B., Wilson, T., Brown, A., Bordoni, A., Willis, M., Khan, S.A., Rovira-Navarro, M., Dalziel, I.W.D., Smalley, R., Kendrick, E., Konfal, S., Caccamise, D.J., Aster, R.C., Nyblade, A., and Wiens, D.A.: Observed rapid bedrock uplift in Amundsen Sea Embayment promotes ice-sheet stability, Science, 360, 1335–1339, https://doi.org/10.1126/science.aao1447, 2018.

Becker, T.W., and Boschi, L.: A comparison of tomographic and geodynamic mantle models, Geochem. Geophys. Geosyst., 3, https://doi.org/10.1029/2001GC000168, 2002.

Berends, C.J., Goelzer, H., Reerink., T.J., Stap., L.B., and van de Wal, R.S.W.: Benchmarking the vertically integrated ice-sheet model IMAU-ICE (version 2.0), Geosci. Model Dev., 15, 5667–5688, https://doi.org/10.5194/gmd-15-5667-2022, 2022.

Blank, B., Barletta, V., Hu, H., Pappa, F., and van der Wal, W.: Effect of lateral and stress-dependent viscosity variations on GIA induced uplift rates in the Amundsen Sea Embayment. *Geochemistry, Geophysics, Geosystems*, *22*(9), https://doi.org/10.1029/2021GC009807, 2021.

Book, C., Hoffman, M.J., Kachuck, S.B., Kachuck, S.B., Hillebrand, T.R., Price, S.F., Perego, M., and Bassis, J.N.: Stabilizing effect of bedrock uplift on retreat of Thwaites Glacier, Antarctica, at centennial timescales, Earth Planet. Sci. Lett., 597, 117798, https://doi.org/10.1016/j.epsl.2022.117798, 2022.

Bueler, E., and Brown, J.: Shallow shelf approximation as a "sliding law" in a thermomechanically coupled ice sheet model, J. Geophys. Res.-Earth, 114, F03008, https://doi.org/10.1029/2008JF001179, 2009.

Bulthuis, K., Arnst, M., Sun, S., and Pattyn, F.: Uncertainty quantification of the multi-centennial response of the Antarctic Ice Sheet to climate change, The Cryosphere, 13, 1349–1380, https://doi.org/10.5194/tc-13-1349-2019, 2019.

heeft verwijderd:

heeft verwijderd: ice sheet

Coulon, V., Bulthuis, K., Whitehouse, P. L., Sun, S., Haubner, K., Zipf, L., and Pattyn, F.: Contrasting response of West and East Antarctic Ice Sheets to glacial isostatic adjustment, J. Geophys. Res.-Earth Surf., 126, e2020JF006003, https://doi.org/10.1029/2020JF006003, 2021.

Coulon, V., Klose, A., Kittel, C., Edwards, T., Turner, F., Winkelmann, R., and Pattyn, F.: Disentangling the drivers of future Antarctic ice loss with a historically calibrated ice-sheet model, The Cryosphere, 18, 653–681, https://doi.org/10.5194/tc-18-653-2024, 2024.

Christensen, U.: Convection with pressure- and temperature-dependent non-Newtonian rheology, Geophys. J. Int., 77, 343–384, https://doi.org/10.1111/j.1365-246X.1984.tb01939.x, 1984.

Danabasoglu, G., Lamarque, J.-F., Bacmeister, J., Bailey, D. A., DuVivier, A. K., Edwards, J., et al.: The Community Earth System Model Version 2 (CESM2). *Journal of Advances in Modeling Earth Systems*, 12, doi:10.1029/2019MS001916, 2020.DeConto, R.M., Pollard, D., Alley, R.B., Velicogna, I., Gasson, E., Gomez, N., Sadai, S., Condron, A., Gilford, D.M., Ashe, E.L., Kopp, R.E., Li, D., and Dutton, A.: The Paris Climate Agreement and future sea-level rise from Antarctica, Nature, 593, 83–89, https://doi.org/10.1038/s41586-021-03427-0, 2021.

Eyring, V., Bony, S., Meehl, G. A., Senior, C. A., Stevens, B., Stouffer, R. J., and Taylor, K. E.: Overview of the Coupled Model Intercomparison Project Phase 6 (CMIP6) experimental design and organization, Geosci. Model Dev., 9, 1937–1958, https://doi.org/10.5194/gmd-9-1937-2016, 2016.

Farrell, W.E., and Clark, J.A.: On Postglacial Sea Level, Geophys. J. R. Astron. Soc., 46, 647–667, https://doi.org/10.1111/j.1365-246X.1976.tb01252.x, 1976.

Favier, L., Jourdain, N.C., Jenkins, A., Merino, N., Durand, G., Gagliardini, O., Gillet-Chaulet, F., and Mathiot, P.: Assessment of sub-shelf melting parameterisations using the ocean–ice-sheet coupled model NEMO(v3.6)–Elmer/Ice(v8.3), Geosci. Model Dev., 12, 2255–2283, https://doi.org/10.5194/gmd-12-2255-2019, 2019.

Fox-Kemper, B., Hewitt, H.T., and Xiao, C.: Ocean, Cryosphere and Sea Level Change, in: Climate Change 2021: The Physical Science Basis. Contribution of Working Group I to the Sixth Assessment Report of the Intergovernmental Panel on Climate Change, Cambridge University Press, 1211–1362, https://doi.org/10.1017/9781009157896.011, 2021.

Golledge, N., Kowalewski, D., Naish, T., Levy, R.H., Fogwill, C.J., and Gasson, E.G.W.: The multi-millennial Antarctic commitment to future sea-level rise. Nature, 526, 421–425, https://doi.org/10.1038/nature15706, 2015.

Golledge, N.R., Keller, E.D., Gomez, N., Naughten, K.A., Bernales, J., Trusel, L.D., and Edwards, T.L.: Global environmental consequences of twenty-first-century ice-sheet melt, Nature, 566, 65–72, https://doi.org/10.1038/s41586-019-0889-9, 2019.

Gomez, N., Pollard, D., and Holland, D.: Sea-level feedback lowers projections of future Antarctic Ice-Sheet mass loss, Nat. Commun., 6, 8798, https://doi.org/10.1038/ncomms9798, 2015.

Gomez, N., Yousefi, M., Pollard, D., DeConto, R. M., Sadai, S., Lloyd, A., Nyblade, A., Wiens, D.A., Aster, R.C., and Wilson, T.: The influence of realistic 3D mantle viscosity on Antarctica's contribution to future global sea levels, Sci. Adv., 10(31), eadn1470, https://doi.org/10.1126/sciadv.adn1470, 2024.

heeft verwijderd: ice sheets

Heeszel, D.S., Wiens, D.A., Anandakrishnan, S., Aster, R.C., Dalziel, I.W.D., Hierta, A.D., Nyblade, A.A., Wilson, T.J., and Winberry, J.P.: Upper Mantle Structure of Central and West Antarctica from Array Analysis of Rayleigh Wave Phase Velocities, J. Geophys. Res.-Sol. Ea., 121, 1758–1775, https://doi.org/10.1002/2015JB012616, 2016.

Hirth, G., and Kohlstedt, D. L.: Rheology of the Upper Mantle and the Mantle Wedge: A View from the Experimentalists, in: Inside the Subduction Factory, edited by: Eiler, J., American Geophysical Union, Washington, D. C., USA, 83–105, https://doi.org/10.1029/138GM06, 2003.

Ivins, E. R., van der Wal, W., Wiens, D. A., Lloyd, A. J., and Caron, L.: Antarctic upper mantle rheology, in: The Geochemistry and Geophysics of the Antarctic Mantle, edited by: Martin, A. P. and van der Wal, W., https://doi-org.utrechtuniversity.idm.oclc.org/10.1144/M56-2020-19, 2023.

Jamieson, T.F. On the history of the last geological changes in Scotland. Quarterly Journal of the Geological Society, London, 21, 161–204, https://doi.org/10.1144/gsl.Jgs.1865.021.01-02.24, 1865.

Kachuck, S. B., Martin, D. F., Bassis, J. N., and Price, S. F.: Rapid viscoelastic deformation slows marine ice sheet instability at Pine Island Glacier, Geophys. Res. Lett., 47, e2019GL086446, https://doi.org/10.1029/2019GL086446, 2020.

Kaufmann, G., Wu, P., and Ivins, E. R.: Lateral viscosity variations beneath Antarctica and their implications on regional rebound motions and seismotectonics, J. Geodyn., 39(2), 165–181, https://doi.org/10.1016/j.jog.2004.08.009, 2005.

Klose, A. K., Coulon, V., Pattyn, F., and Winkelmann, R.: The long-term sea-level commitment from Antarctica, The Cryosphere, 18, 4463–4492, https://doi.org/10.5194/tc-18-4463-2024, 2024.

Konrad, H., Sasgen, I., Pollard, D., and Klemann, V..: Potential of the solid-Earth response for limiting long-term West Antarctic Ice Sheet retreat in a warming climate, Earth Planet. Sci. Lett., 432, 254–264, https://doi.org/10.1016/j.epsl.2015.10.008, 2015.

LeMeur, E., and Huybrechts, P.: A comparison of different ways of dealing with isostasy: examples from modelling the Antarctic Ice Sheet during the last glacial cycle, Ann. Glaciol., 23, 309–317, https://doi.org/10.3189/S0260305500013586, 1996.

Levermann, A., Winkelmann, R., Albrecht, T., Goelzer, H., Golledge, N. R., Greve, R., Huybrechts, P., Jordan, J., Leguy, G., Martin, D., Morlighem, M., Pattyn, F., Pollard, D., Quiquet, A., Rodehacke, C., Seroussi, H., Sutter, J., Zhang, T., Van Breedam, J., Calov, R., DeConto, R., Dumas, C., Garbe, J., Gudmundsson, G. H., Hoffman, M. J., Humbert, A., Kleiner, T., Lipscomb, W. H., Meinshausen, M., Ng, E., Nowicki, S. M. J., Perego, M., Price, S. F., Saito, F., Schlegel, N.-J., Sun, S. and van de Wal, R. S. W.: Projecting Antarctica's contribution to future sea-level rise from basal ice shelf melt using linear response functions of 16 ice sheet models (LARMIP-2), Earth Syst. Dynam., 11(1), 35–76, https://doi.org/10.5194/esd-11-35-2020, 2020.

Lloyd, A.J., Wiens, D.A., Zhu, H., Tromp, J., Nyblade, A.A., Aster, R.C., Hansen, S.E., Dalziel, I., Wilson, T., Ivins, E.R., and O'Donnell, J.P.: Seismic structure of the Antarctic upper mantle imaged with adjoint tomography, J. Geophys. Res.-Sol. Ea., 124, 1115–1130, https://doi.org/10.1029/2019JB017823, 2019.

heeft verwijderd: ice sheet

heeft verwijderd:

Lurton, T., Balkanski, Y., Bastrikov, V., Bekki, S., Bopp, L., Braconnot, P., et al.: Implementation of the CMIP6 forcing data in the IPSL-CM6A-LR model. *Journal of Advances in Modeling Earth Systems*, 12, doi:10.1029/2019MS001940, 2020.

McConnell, R.K.: Viscosity of the mantle from relaxation time spectra of isostatic adjustment, J. Geophys. Res., 70, 5171–5188, https://doi.org/10.1029/JZ070i020p05171, 1965.

Morland, L.W.: Unconfined ice-shelf flow, in: Dynamics of the West Antarctic Ice Sheet, edited by: Van der Veen, C. J., Oerlemans, J., D. Reidel Publishing Company, Dordrecht, the Netherlands, 99–116, https://doi.org/10.1007/978-94-009-3745-1, 1985.

Morlighem, M., Rignot, E., Binder, T. *et al.*: Deep glacial troughs and stabilizing ridges unveiled beneath the margins of the Antarctic Ice Sheet, Nat. Geosci., 13, 132–137, https://doi.org/10.1038/s41561-019-0510-8, 2020.

Milne, G.A., Mitrovica, J.X., Davis, J.L.: Near-field hydro-isostasy: the implementation of a revised sea-level equation, *Geophysical Journal International*, 139, 2, 464–482, https://doi.org/10.1046/j.1365-246x.1999.00971.x, 1999.

Mitrovica, J.X., Gomez, N., Morrow, E., Hay, C., Latychev, K., and Tamisiea, M.E.: On the robustness of predictions of sea level fingerprints, *Geophysical Journal International*, 187, 729–742, https://doi.org/10.1111/j.1365-246X.2011.05090.x, 2011.

Oude Egbrink, D.F.: Modelling the Last Glacial Ice Sheet on Antarctica with Laterally Varying Relaxation Time, MSc Thesis, Delft University of Technology, Delft, the Netherlands, 2018.

Pappa, F., Ebbing, J., Ferraccioli, F. and van der Wal, W.: Modeling satellite gravity gradient data to derive density, temperature, and viscosity structure of the Antarctic lithosphere. *Journal of Geophysical Research: Solid Earth*, 124(11), 12053-12076, 10.1029/2019JB017997, 2019.

Paulson, A., Zhong, S., and Wahr, J.: Modelling post-glacial rebound with lateral viscosity variations, Geophys. J. Int., 163, 357–371, https://doi.org/10.1111/j.1365-246X.2005.02645.x, 2005.

Peltier, W. R.: The impulse response of a Maxwell Earth. *Reviews of Geophysics*, *12*(4), 649-669, https://doi.org/10.1029/RG012i004p0064, 1974.

Peltier, W.R.: Glacial-Isostatic Adjustment—II. The Inverse Problem, Geophys. J. Int., 46, 669–705, https://doi.org/10.1111/j.1365-246X.1976.tb01253.x, 1976.

Pollard, D., Gomez, N., and DeConto, R.M.: Variations of the Antarctic Ice Sheet in a coupled ice sheet-Earth-sea level model: Sensitivity to viscoelastic Earth properties, J. Geophys. Res.-Earth Surf., 122(11), 2124–2138, https://doi.org/10.1002/2017JF004371, 2017.

Ritsema, J., van Heijst, H.J., and Woodhouse, J.H.: Complex shear wave velocity structure imaged beneath Africa and Iceland, Geophys. J. Int., 184, 1223–1236, https://doi.org/10.1126/science.286.5446.1925, 2011.

Rodehacke, C.B., Pfeiffer, M., Semmler, T., Gurses, O., and Kleiner, T.: Future sea level contribution from Antarctica inferred from CMIP5 model forcing and its dependence on precipitation ansatz, Earth Syst. Dynam., 11(4), 1153–1194, https://doi.org/10.5194/esd-11-1153-2020, 2020.

heeft verwijderd: ice sheet

Schaeffer, A.J., and Lebedev, S.: Global shear speed structure of the upper mantle and transition zone, Geophys. J. Int., 194, 417–449, https://doi.org/10.1093/gji/ggt095, 2013.

Seroussi, H., Nowicki, S., Payne, A.J., Goelzer, H., et al.: ISMIP6 Antarctica: a multi-model ensemble of the Antarctic Ice Sheet evolution over the 21st century, The Cryosphere Discuss., https://doi.org/10.5194/tc-2019-324, 2020.

Seroussi, H., Pelle, T., Lipscomb, W.H., Abe-Ouchi, A., et al.: Evolution of the Antarctic Ice Sheet over the next three centuries from an ISMIP6 model ensemble, Earth's Future, 12, https://doi.org/10.1029/2024EF004561, 2024.

Turcotte, D.L., and Schubert, G.: Geodynamics, 2nd edn., Cambridge University Press, Cambridge, United Kingdom, 2002.

van Calcar, C.J., van de Wal, R.S.W., Blank, B., de Boer, B., and van der Wal, W.: Simulation of a fully coupled 3D glacial isostatic adjustment – ice sheet model for the Antarctic Ice Sheet over a glacial cycle, Geosci. Model Dev., 16, 5473–5492, https://doi.org/10.5194/gmd-16-5473-2023, 2023.

van Calcar, C. J., Bernales, J., Berends, C.J., van de Wal, R.S.W., and van der Wal, W.: Assessing the interaction between ice dynamics, sub-shelf melt and GIA over a glacial cycle using a fully coupled GIA-ice sheet model. Preprint, 2024.

van Calcar, C. J., Bernales, J., Berends, C.J., van de Wal, R.S.W., and van der Wal, W.: Bedrock uplift reduces Antarctic sea-level contribution over next centuries. Preprint, https://doi.org/10.21203/rs.3.rs-4863941/v1, 2024.

van der Wal, W., Whitehouse, P. L., and Schrama, E. J. O.: Effect of GIA models with 3D composite mantle viscosity on GRACE mass balance estimates for Antarctica, Earth Planet. Sci. Lett., 414, 134–143, https://doi.org/10.1016/j.epsl.2015.01.001, 2015.

van der Wal, W., Barnhoorn, A., Stocchi, P., Gradmann, S., Wu, P., Drury, M., and Vermeersen, B.: Glacial isostatic adjustment model with composite 3-D Earth rheology for Fennoscandia, *Geophysical Journal International*, 194, 61–77, https://doi.org/10.1093/gji/ggt099, 2013.

Wan, J. X. W., Gomez, N., Latychev, K., and Han, H. K.: Resolving glacial isostatic adjustment (GIA) in response to modern and future ice loss at marine grounding lines in West Antarctica, The Cryosphere, 16, 2203–2223, https://doi.org/10.5194/tc-16-2203-2022, 2022.

Wang, H., and Wu, P.: Effects of lateral variations in lithospheric thickness and mantle viscosity on glacially induced relative sea levels and long wavelength gravity field in a spherical, self-gravitating Maxwell Earth, Earth Planet. Sci. Lett., 249(3–4), 368–383, https://doi.org/10.1016/j.epsl.2006.07.011, 2006.

Whitehouse, P., Gomez, N., King, M. A., and Wiens, D. A.: Solid Earth change and the evolution of the Antarctic Ice Sheet, Nat. Commun., 10, 503, https://doi.org/10.1038/s41467-018-08068-y, 2019.

Whitehouse, P. L., Latychev, K., Milne, G. A., Mitrovica, J. X., and Kendall, R.: Impact of 3-D Earth structure on Fennoscandian glacial isostatic adjustment: Implications for space-geodetic estimates of present-day crustal deformations, Geophys. Res. Lett., 33, L13502, https://doi.org/10.1029/2006GL026568, 2006.

Wu, P., and Peltier, W. R.: Viscous gravitational relaxation, Geophys. J. Int., 70, 435–485, https://doi.org/10.1111/j.1365-246X.1982.tb04976.x, 1982.

heeft verwijderd: ice sheet

heeft verwijderd:

heeft verwijderd: ice sheet

heeft verwijderd:

Wu, P. and Johnston, P.: Validity of Using Flat-Earth Finite Element Models in the Study of Postglacial Rebound, in: Dynamics of the Ice Age Earth, edited by: Wu, P., Trans Tech Publications Ltd, Switzerland, 191–202, 1998.

Wu, P.: Sensitivity of relative sea levels and crustal velocities in Laurentide to radial and lateral viscosity variations in the mantle, Geophys. J. Int., 165, 401–413, https://doi.org/10.1111/j.1365-246X.2006.02960.x, 2006.

Wu, P., and van der Wal, W.: Postglacial sealevels on a spherical, self-gravitating viscoelastic earth: Effects of lateral viscosity variations in the upper mantle on the inference of viscosity contrasts in the lower mantle, Geophys. J. Int., 192, 7–17, https://doi.org/10.1016/S0012-821X(03)00199-7, 2013.

Zhao, C., King, M. A., Watson, C. S., Barletta, V. R., Bordoni, A., Dell, M., and Whitehouse, P. L.: Rapid ice unloading in the Fleming Glacier region, southern Antarctic Peninsula, and its effect on bedrock uplift rates, Earth Planet. Sci. Lett., 473, 164–176, https://doi.org/10.1016/j.epsl.2017.06.002, 2017.

Zoet, L. K., and Iverson, N. R.: A slip law for glaciers on deformable beds, Science, 368(6486), 76–78, https://doi.org/10.1126/science.aaz1183, 2020.